DALTON
FULL PAPER

Studies on *ansa*-zirconocene–butadiene derivatives

Jennifer C. Green, Malcolm L. H. Green, Grant C. Taylor and John Saunders

Inorganic Chemistry Laboratory, South Parks Road, Oxford, UK OX1 3QR

Received 26th October 1999, Accepted 14th December 1999

The new compounds [Zr{$Me_2C(\eta\text{-}C_5H_4)_2$}(*cis*-$\eta\text{-}C_4H_6$)] (**2***), [Zr{$Me_2C(\eta\text{-}C_5H_4)_2$}$Ph_2$] (**3**), [Zr{$Me_2C(C_5H_4)_2$}(*cis*-$\eta^4$-$C_4H_4Me_2$)] (**4***), [Zr{$Me_2C(\eta\text{-}C_5H_4)_2$}(*cis*-$\eta^4$-$PhC_4H_4Ph$)] (**5**), [Zr{$Me_2C(\eta\text{-}C_5H_4)_2Cl$}$_2$-μ-O] (**6***), [Zr{$Me_2C(\eta\text{-}C_5H_4)_2$}{$\eta^3$-$C_4H_6B(C_6F_5)_3$}] (**7**), [Zr{$Me_2C(\eta\text{-}C_5H_4)_2$}{*exo*-$\eta^3$-$C_4H_6B(C_6F_5)_3$}$PMe_3$] (**8***), [Zr{$Me_2C(\eta\text{-}C_5H_4)_2$}{*endo*-$\eta^3$-$C_4H_6B(C_6F_5)_3$}$C_6H_5N$] (**9***), and [Zr{$Me_2C(\eta\text{-}C_5H_4)_2$}{*endo*- and *exo*-$\eta^3$-$C_4H_6B(C_6F_5)_3$}NC′Bu] (**10a**) and (**10b**) have been prepared. An asterisk indicates the crystal structure has been determined. The photoelectron spectra of **2** and **4** have been determined and assigned with the assistance of density functional methods. The factors relating to the relative stability of *cis*- and *trans*-butadiene structures for **2** and **4** are discussed.

We have been interested to explore the stereo-electronic effects of the presence of *ansa*-bridging groups in *ansa*-metallocenes compared to those of their non-*ansa* analogues.[1–4] In this work we have investigated *ansa*-zirconocenes. Erker and co-workers[5–7] and Nakamura *et al.*[8] have previously carried out elegant and detailed studies of Group IV metallocene–butadiene derivatives. In particular they have shown that the η-butadiene ligand in compounds such as [$Zr(\eta\text{-}C_5H_5)_2$(*trans*-$\eta\text{-}C_4H_6$)] adopts the rare *trans* geometry when coordinated to the zirconium centre. The NMR data indicates there is an equilibrium between the more stable *trans*- and the less stable *cis*-configurations.[9] The underlying reasons for the relative stability of the two coordination models have been investigated by Extended Huckel calculations.[10] We were interested to study the effect of an *ansa*-bridge on this equilibrium.

Results and discussion

The *ansa*-zirconocene [Zr{$Me_2C(\eta\text{-}C_5H_4)_2$}$Cl_2$] (**1**)[11] was treated with a suspension of butadiene magnesium[12] in toluene at 0 °C to give [Zr{$Me_2C(\eta\text{-}C_5H_4)_2$}(*cis*-$\eta\text{-}C_4H_6$)] (**2**) in 90% yield. Large crystals of **2** were formed from toluene at −25 °C. The crystal structure was determined and the molecular structure is shown in Fig. 1 and selected distances and angles are listed in Table 1. The compound **2** crystallises in a monoclinic crystal system with the space group $P2_1/n$. The unit cell contains two independent crystallographic units. Hydrogen atoms on the butadiene ligand were located experimentally, whilst hydrogen atoms on the bis-cyclopentadienyl ligand were placed in calculated positions. The structure clearly shows that the η-butadiene moiety in **2** adopts a *cis* disposition whilst acting as a four-electron ligand. Some metallocyclopentene character is

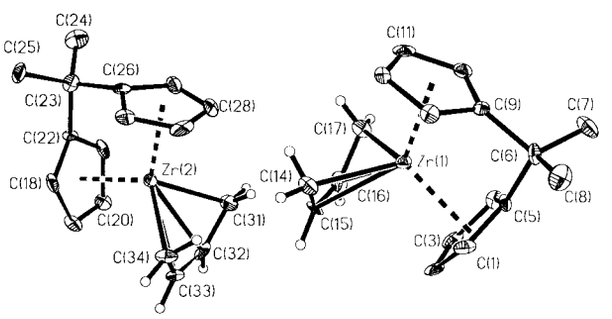

Fig. 1 Molecular structure of compound [Zr{$Me_2C(\eta\text{-}C_5H_4)_2$}(*cis*-$\eta\text{-}C_4H_6$)] **2**.

Table 1 Selected interatomic distances (Å) and angles (°) for [Zr{$Me_2C(\eta\text{-}C_5H_4)_2$}(*cis*-$\eta\text{-}C_4H_6$)] **2**

Zr–C(14)	2.313(6)	Zr–C(14)–H_{anti}	98.02
Zr–C(15)	2.461(6)	Zr–C(14)–H_{syn}	141.55
C(14)–C(15)	1.436(7)	Zr–C(14)–C(15)	78.2(4)
C(15)–C(16)	1.370(8)	H_{anti}–C(14)–H_{syn}	107
C(14)–H_{anti}	0.91	H_{anti}–C(14)–C(15)	114
C(14)–H_{syn}	0.88	H_{syn}–C(14)–C(15)	112
Zr–H_{anti}	2.65	C(14)–C(15)–C(16)	126.4(5)
Zr–H_{syn}	3.12	(CEN)–Zr(CEN)	114.5

indicated by the shorter C(15)–C(16) bond distance of 1.370(8) Å compared with the 1.436(7) Å between the C(14)–C(15) carbons implying some double bond character between the atoms. Further, the terminal carbon atoms of the butadiene fragment, which have a distorted tetrahedral coordination, imply sp^3 hybridisation and thus significant σ-donation to the metal. The *anti*-hydrogens of the butadiene moiety are tilted towards the metal centre, the Zr–C–H angle being 98°, bringing these protons within 2.6 Å of the zirconium centre. This distance is too long to invoke the presence of agostic bonding.

The ^{1}H NMR spectra of compound **2** have been determined over the range −90 °C to +95 °C. The analytical and NMR data for **2**, and for all the other new compounds described in this work are given in Table 2. The presence of only four separate cyclopentadienyl resonances, at values of δ 4.66, 4.89, 5.09, and 5.62, confirms that the structure of the η-butadiene ligand is rigid on the NMR timescale and the spectrum corresponds to a molecule which possesses only one mirror plane or C_2 axis. We conclude that it appears that the *ansa*-bridge somehow restricts the butadiene ligand from flipping between the *cis*- and *trans*-structures. The smaller bite angle of the *ansa*-bridged ligand leaves more room in the coordination sphere of the metal for such rearrangement processes of the butadiene ligand so an explanation in electronic terms seems more likely.

Treatment of a THF solution of [Zr{$Me_2C(\eta\text{-}C_5H_4)_2$}$Cl_2$] with two equivalents of phenylmagnesium bromide gave beige microcrystals which the NMR data suggest are the compound [Zr{$Me_2C(\eta\text{-}C_5H_4)_2$}$Ph_2$] (**3**). These crystals decomposed slowly in the presence of light to a pink substance so manipulations were performed in the dark. The compound **3** was not characterised but was immediately further reacted. A suspension of **3** in toluene was treated with an excess of freshly distilled 2,3-dimethylbutadiene and the mixture was irradiated with uv light for 15 h. During this period the reaction mixture turned red-orange. The proton NMR spectrum of the unpurified product indicated the presence of a mixture of

Table 2 Analytical and spectroscopic data

Compound	Colour	Analysis (%)[a] C	H	N	Cl	P	Zr	NMR data[b]
[Zr{Me_2C(η-C_5H_4)$_2$}-(*cis*-η-C_4H_6)] **2**[c]	Deep red	64.8 (63.6)	6.3 (6.3)	—	—	—	28.8 (30.8)	^{1}H[d,e]: 5.62 (t 2H) H_{Cp}, 5.09 (t 2H) H_{Cp}, 4.89 (t 2H) H_{Cp}, 4.845 (m 2H) H_{meso}, 4.658 (t 2H) H_{Cp}, 3.517 (m 2H) H_{syn}, 1.425 (s 6H) CH_3, 0.915 (m 2H) H_{anti}. ^{13}C{^{1}H}[e]: 111.5 C_b, 108.6 Cp CH, 51.7 C_a, 102.7 Cp CH, 101.4 Cp CH, 89.2 Cp CH, 24.3 CH_3, quaternary C not seen; CH connectivities were confirmed by HSQC analysis.
[Zr{Me_2C(η-C_5H_4)$_2$}-Ph_2] **3**	Beige	—	—	—	—	—	—	^{1}H[f]: 7.49 (m 4H), 7.21 (m 4H), 7.15 (m 2H) C_6H_5-, 6.18 (m 4H), 5.34 (m 4H), 1.20 (s 6H) CMe_2. ^{13}C[f]: 135.5, 126.7, 126.5 C_6H_5-, 116.8, 106.7 Cp CH's. ^{13}C signals were indirectly detected and so quaternary carbon atoms were not observed.
[Zr{$Me_2C(C_5H_4)_2$}-(*cis*-η^4-$C_4H_4Me_2$)] **4**	Deep red	60.4 (66.4)[i]	7.2 (7.0)	—	—	—	24.5 (26.55)	^{1}H[f,g]: 5.64 (m 2H) Cp CH, 5.29 (m 2H) Cp CH, 5.09 (m 2H) Cp CH, 4.89 (m 2H) Cp CH, 3.43 (d 2H) H_{syn}, 1.84 (s 6H) butadiene CH_3, 1.47 (s 6H) CMe_2, −0.86 (d 2H) H_{anti}. ^{13}C{^{1}H}[f]: 119.7 C_b, 108.7 Cp CH, 104.7 Cp CH, 102.4 Cp CH, 91.1 Cp CH, 58.1 C_a, 35.7 *C*Me_2, 24.44 CMe_2 or butadiene CH_3, 24.36 CMe_2 or butadiene CH_3. Cp quaternary C not seen. CH connectivities were assigned by an HSQC experiment.
[Zr{Me_2C(η-C_5H_4)$_2$}-(*cis*-η^4-PhC_4H_4Ph)] **5**	Deep red[i]	—	—	—	—	—	—	^{1}H[d,f]: 7.30 (m 4H) C_6H_5-, 7.20 (m 2H) C_6H_5-, 7.05 (m 4H) C_6H_5-, 5.50 (dm 2H) H_b, 5.22 (m 2H) Cp CH, 5.10 (m 2H) Cp CH, 5.00 (m 2H) Cp CH, 4.53 (m 2H) Cp CH, 1.18 (dm 2H) H_a, 1.08 (s 6H) CMe_2. ^{13}C[f]: 128.9 C_6H_5-, 126.6 C_6H_5-, 122.3 C_6H_5-, 110.8 Cp CH, 105.4 Cp CH, 104.9 Cp CH, 92.7 Cp CH, 23.5 CMe_2, 23.2 C_a. ^{13}C signals were indirectly detected and so quaternary carbon was not observed. ^{1}H assignments were made by DQF COSY analysis.
[Zr{Me_2C(η-C_5H_4)$_2$-Cl}$_2$-μ-O] **6**	Colourless	52.5 (52.6)	5.0 (4.75)	—	9.9 (11.6)	—	27.6 (30.7)	^{1}H[f]: 6.50 (m 2H) Cp CH, 6.37 (m 2H) Cp CH, 5.61 (m 2H) Cp CH, 5.28 (m 2H) Cp CH, 1.35 (s 3H) CMe_2, 1.23 (s 3H) CMe_2. ^{13}C{^{1}H}[f]: 126.6 Cp C_{quat}, 120.5 Cp CH, 118.0 Cp CH, 105.9 Cp CH, 104.5 Cp CH, 37.5 *C*Me_2, 24.3 CMe_2, 23.8 CMe_2.
[Zr{Me_2C(η-C_5H_4)$_2$}-{η^3-$C_4H_6B(C_6F_5)_3$}] **7**	Orange	50.6 (50.8)	2.2 (2.4)	—	—	—	10.6 (11.0)	^{1}H[e,g]: 5.70 (m 1H) CpCH, 5.27 (m 1H) H_b, 5.21 (m 1H) CpCH, 5.19 (m 1H) Cp′CH, 5.16 (m 1H) Cp′CH, 5.06 (m 1H) CpCH, 4.77 (m 1H) Cp′CH, 4.66 (m 1H) CpCH, 4.55 (m 1H) H_c, 4.09 (m 1H) Cp′CH, 2.73 (m 1H) H_a, 1.09 (s 3H) CMe_2, 0.97 (s 3H) CMe_2, 0.94 (m 1H) $H_{a'}$, −0.25 (m br 1H) $H_{d_{anti}}$, −1.13 (m br 1H) $H_{d_{syn}}$. ^{13}C[e]: 133.2 C_b, 116.4 CpCH, 112.0 Cp′CH, 111.6 CpCH, 111.5 C_c, 108.7 Cp′CH, 106.2 Cp′CH, 105.4 Cp′CH, 96.4 CpCH, 92.8 CpCH, 56.3 C_a, 26.2 C_d, 23.0 CMe_2, 22.9 CMe_2. ^{19}F[e] at 294 K: −135.9 (d *ortho*-F), −162.2 (t *para*-F), −167.5 (br t *meta*-F). ^{11}B{^{1}H} (160 MHz C_7D_8): −12.66 s. ^{1}H assignments were made by DQF COSY analysis. ^{13}C signals were indirectly detected and assigned by HSQC experiments, and so quaternary carbon signals were not observed.
[Zr{Me_2C(η-C_5H_4)$_2$}-{*exo*-η^3-C_4H_6B-$(C_6F_5)_3$}PMe_3] **8**	Pale yellow	51.1 (50.5)	3.3 (3.2)	—	—	3.4 (3.4)	—	^{1}H[g,h]: 6.30 (m 2H) Cp CH, 6.21 (m 2H) Cp CH, 5.95 (m 4H) Cp CH, 5.72 (m 1H) H_b, 4.53 (dm 1H) H_a, 4.32 (dm 1H) H_a, 1.94 (d 9H) PMe_3, 1.86 (m) $H_{d_{anti}}$, 1.83 (s 3H) CMe_2, 1.79 (s 3H) CMe_2, 1.52 (t 1H) H_c, 1.18 (d 1H) $H_{d_{syn}}$. ^{13}C[h]: 143 C_b, 132.1 CpC_{quat}, 132.0 CpC_{quat}, 117.2 CpCH, 117.0 CpCH, 115.5 CpCH, 114.9 CpCH, 112.9 C_a, 103.8 CpCH, 103.7 CpCH, 103.4 Cp CH, 103.3 CpCH, 55.8 C_c, 37.4 C_d, 25.7 *C*Me_2, 24.7 CMe_2 24.1 CMe_2, 4.7 (d J_{C-P} 53 Hz) PMe_3. ^{13}C signals were assigned by HSQC experiments. ^{1}H assignments were made by DQF COSY analysis. ^{19}F[h]: −133.25 (d *ortho*-F), −169.3 (t *para*-F), −171.8 (br t *meta*-F). ^{31}P{^{1}H}[h]: 33.39 s. ^{11}B{^{1}H}[h]: −13.16 s.

Table 2 (*Contd*)

Compound	Colour	Analysis (%)[a] C	H	N	Cl	P	Zr	NMR data[b]
[Zr{$Me_2C(\eta\text{-}C_5H_4)_2$}-{*endo*-$\eta^3$-$C_4H_6B$-$(C_6F_5)_3$}$C_6H_5N$] **9**	Yellow	54.2 (54.7)	3.9 (3.9)	1.2 (1.3)	—	—	—	^{1}H[g,h]: 8.94 (d 2H) *ortho*-py, 8.40 (t 1H) *para*-py, 7.92 (m 2H) *meta*-py, 6.52 m Cp CH, 6.32 m Cp CH, 5.88 m Cp CH, 5.64 m H_b, 4.53 dm $H_{a'}$, 4.35 dm H_a, 1.72 s CMe_2, 1.62m $H_{d_{anti}}$, 1.58 m H_c, 1.33 m $H_{d_{syn}}$. Assignments were made by DQF-COSY analysis. ^{11}B{^{1}H}[h]: −13.16 s.
[Zr{$Me_2C(\eta\text{-}C_5H_4)_2$}-{*endo*- and *exo*-$\eta^3$-$C_4H_6B(C_6F_5)_3$}NC′Bu] **10a** and **10b**	Pale yellow	53.2 (52.76)	3.2 (3.2)	1.5 (1.5)	—	—	10.0 (10.0)	^{1}H[f,g]: Major isomer: 6.26 H_b, 5.21 (m 1H) Cp CH, 5.11 (m 1H) Cp CH, 5.03 (m 1H) Cp CH, 4.96 (m 1H) Cp CH, 4.79 (m 1H) Cp CH, 4.64 (m 1H) Cp CH, 4.59 (m 1H) Cp CH, 4.21 (m 1H) Cp CH, 3.38 H_a, 2.75 $H_{d_{anti}}$, 1.96 $H_{a'}$, 1.10 H_c, 1.06 (s 9H) Bu^t, 0.96 (s 3H) CMe_2, 0.93 (s 3H) CMe_2, 0.82 $H_{d_{syn}}$. Minor isomer: 5.49 (m 1H) Cp CH, 4.74 (m 2H) Cp CH, 4.69 (m 1H) Cp CH, 4.62 (m 1H) Cp CH, 4.48 (m 1H) Cp CH, 4.38 (m 1H) Cp CH, 4.33 (m 1H) Cp CH, 4.00 H_b, 3.70 H_c, 3.40 $H_{a'}$, 2.00 H_a, 1.69 $H_{d_{anti}}$, 1.03 (s 9H) Bu^t, 1.02 $H_{d_{syn}}$, 0.96 (s 3H) CMe_2, 0.89 (s 3H) CMe_2. ^{19}F[f]: Major isomer: −135.3 d *ortho*-F, −165.1 t *para*-F, −169.1 m *meta*-F. Minor isomer: −135.1 d *ortho*-F, −165.3 t *para*-F, −168.9 m *meta*-F. Proton chemical shifts and assignments were made with the aid of DQF-COSY analysis.

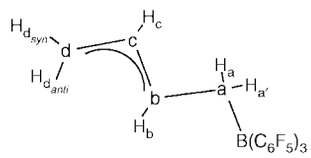

[a] Calculated values are given in parentheses. [b] Data given as chemical shift (δ) (multiplicity, relative intensity) assignment (labelling diagram given above see compound **10a**. [c] MS analysis: *m/z* 315 (molecular ion), 260 $(C_{13}H_{14}Zr)^+$, 54 $(C_4H_6)^+$. [d] At 300 MHz. [e] In perdeuterotoluene. [f] In C_6D_6. [g] At 500 MHz. [h] In $(CD_3)_2CO$. [i] Due to the extreme sensitivity and thermal instability of the solid, satisfactory elemental analysis could not be obtained.

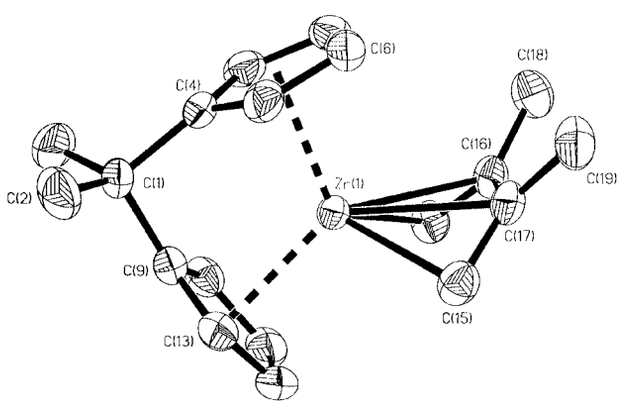

Fig. 2 Molecular structure of compound [Zr{$Me_2C(C_5H_4)_2$}-(*cis*-η^4-$C_4H_4Me_2$)] **4**.

[Zr{$Me_2C(\eta\text{-}C_5H_4)_2$}(*cis*-$\eta$-$C_4H_4Me_2$)] and [Zr{$Me_2C(\eta\text{-}C_5H_4)_2$}$Ph_2$] in an approximate ratio of 5:1. Recrystallisation from THF at −25 °C, giving the pure compound [Zr{$Me_2C(C_5H_4)_2$}(*cis*-η^4-$C_4H_4Me_2$)] (**4**) as large ruby-red crystals. The crystal structure was determined and the molecular structure of **4** is shown in Fig. 2 and selected interatomic distances and angles are given in Table 3.

The molecule **4** crystallises in a triclinic crystal system with a space group $P\bar{1}$. Hydrogen atoms on the butadiene ligand were located experimentally, whilst hydrogens on the bis-cyclopentadienyl ligand were placed in calculated positions. The non-*ansa* analogue of **4** has been described and the predominant isomer has the *cis*-butadiene structure.[9]

The most noticeable difference between the molecular structures of molecules **2** and **4** is that the bonding mode of the butadiene ligand is more metallacyclopentene-like in the latter case. This is reflected by a slight shortening of the zirconium–terminal carbon bond lengths and substantial lengthening of the distance between the metal and the C(17) and C(18) atoms. Indeed the difference in bond lengths between Zr–C(15) and Zr–C(17) increases from 0.148 to 0.261 Å in the case of the

Table 3 Selected interatomic distances (Å) and angles (°) for [Zr-{$Me_2C(C_5H_4)_2$}(*cis*-η^4-$C_4H_4Me_2$)] **4**

Zr–C(15)	2.296(2)	Zr–C(14)–H_{anti}	90.7(19)
Zr–C(17)	2.557(2)	Zr–C(15)–H_{syn}	132.7(19)
C(15)–C(17)	1.450(3)	Zr–C(15)–C(17)	82.8(1)
C(16)–C(17)	1.394(3)	H_{anti}–C(15)–H_{syn}	105.8(35)
C(15)–H_{anti}	0.91(3)	H_{anti}–C(15)–C(17)	116.5(19)
C(15)–H_{syn}	0.94(3)	H_{syn}–C(15)–C(17)	119.2(19)
Zr–H_{anti}	2.485	C(15)–C(17)–C(16)	122.8(2)
Zr–H_{syn}	2.993	CEN–Zr–CEN′	114.2

substituted molecule. The distortion from approximately symmetrical η^4-coordination bends the *anti*-hydrogen even closer to the metal centre. The Zr–C(15)–H_{anti} bond angle decreases by a further 7° to less than 91° bringing the atom to within 2.5 Å of the metal. Comparison of this structure to that of the unbridged *cis*-[Zr(η-C_5H_5)$_2$(η^4-$C_4H_4Me_2$)] analogue[13] shows there are essentially no differences in the bonding in the two metallocyclopentene fragments. However in the absence of the restraining *ansa*-bridge there is an increase in the Cp–Zr–Cp angle from 114° in **4** to 124° in [Zr(η-C_5H_5)$_2$(*cis*-η^4-$C_4H_4Me_2$)]. The proton NMR spectrum of **4** confirms the presence of the *cis*-isomer which, like the unsubstituted analogue, was conformationally rigid on the NMR timescale at ambient temperature.

η-Butadiene ligands require the metal fragment to provide three orbitals and two electrons to bind in an η^4 fashion. In the vast majority of butadiene complexes the diene system adopts a *cis*-configuration since the metal fragment has a trigonal disposition of orbitals suitable for bonding to the diene system. Typical metal fragments are $M(CO)_3$ (M = Fe, Ru, Os) and $M(\eta\text{-}C_5H_5)$ (M = Co, Rh, Ir). The spatial disposition of such a trigonal array is well matched to overlap with the symmetry adapted π-orbitals of *cis*-butadiene.[14] Representations of the orbitals are given in Fig. 3. These orbitals provide good overlap with π_2 and π_3. However when butadiene has the *trans*-configuration, the nodal properties of the π_3 orbital are ill-suited to mix with one of the e orbitals. Bent metallocene

fragments provide three orbitals which are coplanar, see Fig. 3.[15] In this case the $3a_1$ orbital provides a nodal match with π_3 in both the *cis*- and the *trans*-isomers and back donation is possible from the $3a_1$ orbital into π_3. The electron rich nature of zirconocene is likely to make back donation the most important of the bonding interactions.

To investigate further the electronic structure of these complexes we measured the photoelectron (PE) spectra of **2** and **4** and carried out density functional calculations. The photoelectron spectra of **2** and **4** are shown in Fig. 4 and vertical ionisation energies are given in Table 4. The most intense band F is associated with ionisation of the σ-bonding electrons of the cyclopentadienyl ligands. The low energy bands A show little variation in ionisation energy on methyl substitution. Band C is of such an intensity that it appears to comprise several ionisations and occurs in an ionisation region characteristic of the highest occupied p orbitals on the cyclopentadienyl rings. The chief difference between the two spectra is the appearance of band D in the spectrum of **4**. This is presumably associated with the butadiene moiety. Further assignment is best carried out with the aid of the density functional calculations.

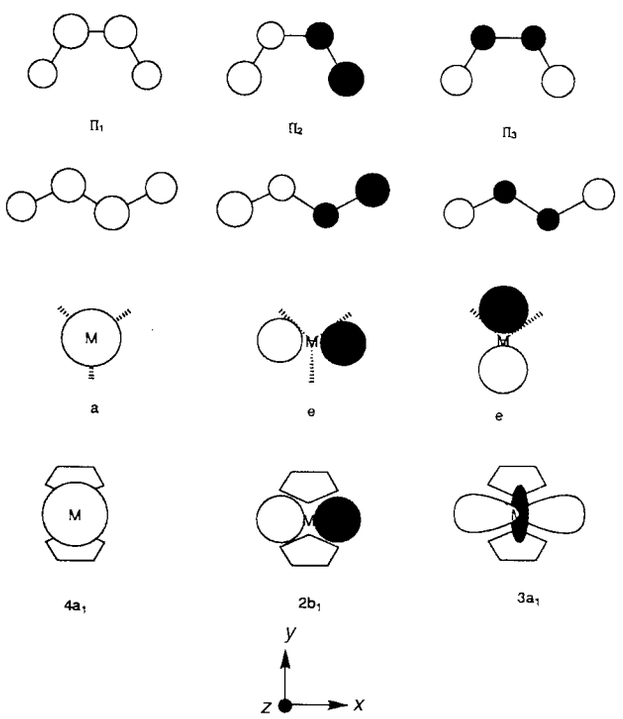

Fig. 3 Representation of the butadiene and metal and frontier orbitals for $Mo(CO)_3$ and $M(Cp_2)$ fragments. The butadiene orbitals are projected onto the plane of the molecule. The metal orbitals are viewed along the principal symmetry axis.

Geometry optimisations were carried out on **2** and **4** assuming C_s symmetry. The resulting bond distances were in good agreement with the X-ray data. Key calculated distances for the Zr–butadiene moieties are compared with the experimental ones in Table 5. Ionisation energies were estimated by calculating energies for the seven lowest ion states. In a few cases SCF convergence was not achieved. The calculated IE are given in Table 4 together with the associated orbital energies in the molecular ground state. Iso-surfaces for key orbitals are given for **2** in Fig. 5.

Band A in both spectra (Fig. 4) is assigned to ionisation from an orbital of metallocene $3a_1$ and butadiene π_3 character. Band B comes from ionising the $2b_2$ orbital of the metallocene fragment; this orbital rises in energy above the other cyclopentadienyl orbitals as the rings are bent. Band C comprises the other cyclopentadienyl ionisations, $1a_2$, $1b_1$ and $2a_1$, together with ionisation from the π_2 orbital mixed with the metallocene $2b_1$ orbital. Band D, only clearly visible in the PE spectrum of **4**, results from ionisation from the π_1 orbital of butadiene. An IE could not be estimated for the comparable orbital of **2** as the associated ion state failed to converge. However, the difference in one electron energies of the associated orbitals suggest that the IE should be about 0.55 eV higher than for **4**, which would place it at the onset of the main band.

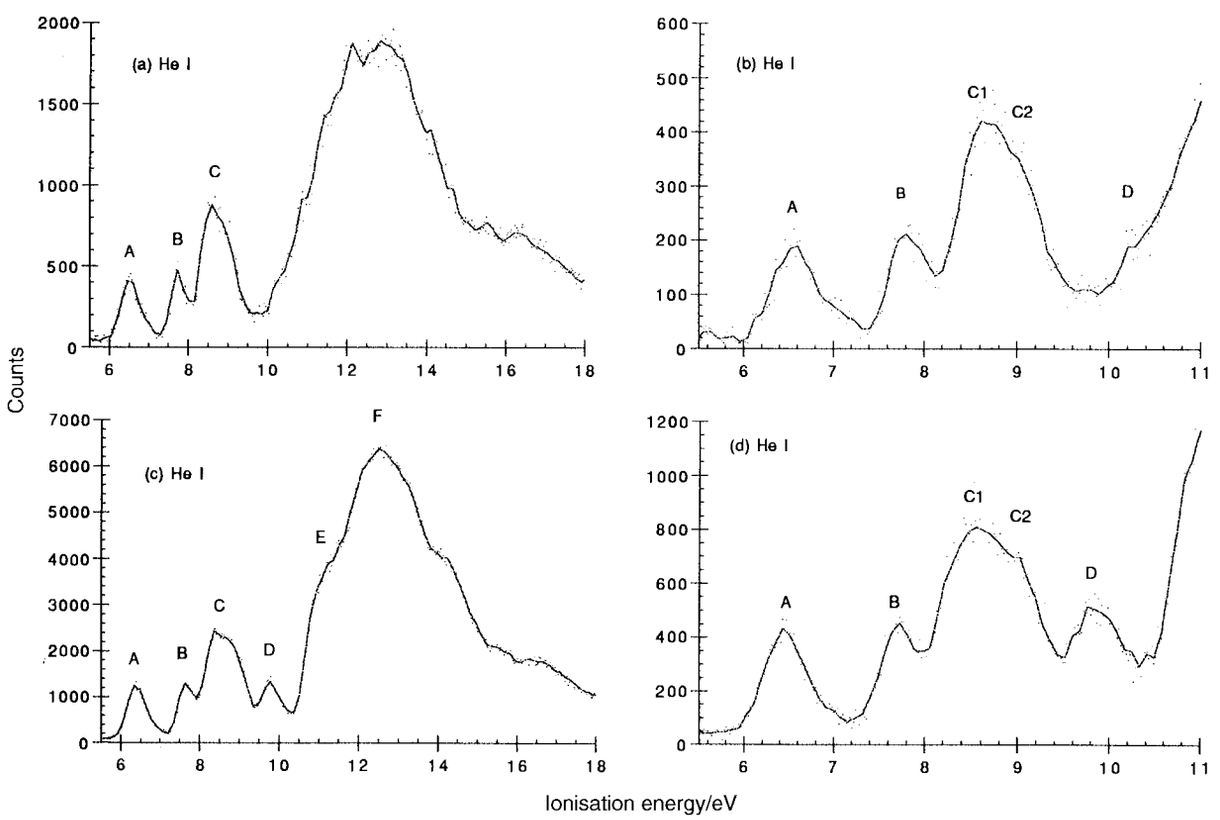

Fig. 4 The photoelectron spectra of **2**, (a) and (b), and **4**, (c) and (d).

Table 4 Experimental and calculated ionisation energies, IE (eV) and assignments for **2** and **4**

2					**4**				
MO	ε	IE calc.	IE exp.	Assignment	MO	ε	IE calc.	IE exp.	Assignment
30a′	−4.09	6.36	6.54 A	$3a_1 + \pi_3$	33a′	−3.92	6.13	6.38 A	$3a_1 + \pi_3$
29a′	−5.39	7.59	7.73 B	$2b_2$	32a′	−5.28	7.46	7.66 B	$2b_2$
20a″	−6.03	8.22		$1a_2$	23a″	−5.85	n.c.[a]		$1a_2$
19a″	−6.10	8.36	8.62 C_1	$\pi_2 + 2b_1$	22a″	−5.98	8.21	8.47 C	$\pi_2 + 2b_1$
18a″	−6.30	8.55	9.00 C_2	$1b_1$	21a″	−6.24	n.c.[a]		$1b_1$
28a′	−6.49	8.69		$2a_1$	31a′	−6.45	8.62		$2a_1$
27a′	−7.66	n.c.[a]	10.3	π_1	30a′	−7.11	9.41	9.80 D	π_1

[a] Not calculated, SCF convergence of ion state was not achieved.

Table 5 Calculated distances and angles for the Zr–butadiene fragment in **2**, **4**, **I**, **II** and **III**; experimental data are given in parentheses

	2	**4**	**I**	**II**	**III**
Zr–C1	2.31 (2.31)	2.29 (2.30)	2.45	2.33	2.45
Zr–C2	2.47 (2.46)	2.52 (2.56)	2.35	2.47	2.38
C1–C2	1.42 (1.44)	1.43 (1.45)	1.41	1.42	1.42
C2–C3	1.39 (1.37)	1.40 (1.39)	1.41	1.39	1.41
Zr–C1–C2	79 (78)	82 (83)	69		
C1–Zr–C4	84	81	95		94

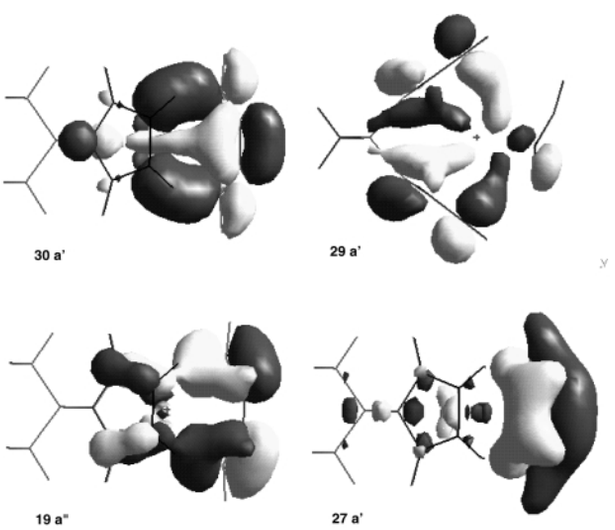

Fig. 5 Iso-surfaces for key bonding orbitals are given for **2**.

The good agreement between calculated and experimental IE lends support to the detailed bonding model revealed by the DFT calculations.

In order to attempt to understand the factors affecting the relative stability of *cis*- and *trans*-modes of binding of the butadiene ligand we also optimised structures of *trans*-[Zr{$Me_2C(\eta$-$C_5H_4)_2$}(η-C_4H_6)], **I**, [Zr(η-$C_5H_5)_2$(*cis*-η-C_4H_6)], **II** and [Zr(η-$C_5H_5)_2$(*trans*-η-C_4H_6)], **III**. Calculated distances and angles for the Zr–butadiene moieties are given in Table 5. In both cases the *cis* isomer was calculated to be more stable than the *trans* but the energies of the two isomers were very close. The energy difference was 7 kJ mol^{-1} in the case of the *ansa*-bridged compounds and 5 kJ mol^{-1} in the case of the unbridged compounds. In contrast the stability of [Fe(*cis*-C_4H_6)$(CO)_3$] relative to [Fe(*trans*-C_4H_6)$(CO)_3$] we calculated as 52 kJ mol^{-1}. Yasuda *et al.*[16] quote a value of 1.3 eV for the energy difference. Thus the equilibrium between *cis*- and *trans*-forms found for [Zr(η-$C_5H_5)_2$(η-C_4H_6)] is well modelled by the calculations; what is less apparent is why only the *cis*-isomer is found for [Zr{$Me_2C(\eta$-$C_5H_4)_2$}(η-C_4H_6)].

Table 6 Occupation of fragment orbitals in Zr butadiene complexes

	π_1	π_2	π_3	$4a_1$	$2b_1$	$3a_1$
2	1.85	1.62	1.19	0.00	0.34	0.73
I	1.85	1.65	1.04	0.04	0.29	0.92
II	1.84	1.60	1.20	0.08	0.37	0.70
III	1.84	1.63	1.06	0.10	0.31	0.90

A fragment analysis was carried out on **2**, **I**, **II** and **III**. Table 6 gives the occupations of the key fragment orbitals illustrated in Fig. 3. The most significant difference is seen between the *cis* and the *trans* complexes, back donation from $3a_1$ to π_3 being more effective in the *cis* configuration than the *trans.* Donation from the π_2 orbital into the $2b_1$ orbital also appears marginally favoured for the *cis* complexes. Donation from π_1 into the $4a_1$ orbital is minimal for all four complexes but appears to be less for the *ansa* bridged compounds than for the unbridged.

We conclude that the non-trigonal and essentially planar nature of the three frontier orbitals used in the bonding of bent zirconocenes to butadiene ligands leads to there being a substantially smaller energy difference between the butadiene ligand adopting *cis*- or *trans*-structures than for the more commonly found *cis*-butadiene–metal compounds with trigonally disposed frontier orbitals. However, the calculations provide no clear explanation for the greater preference for *cis*-butadiene compounds in *ansa*-zirconocenes than in the non-*ansa* analogues.

Recently Burghi *et al.*[17] have investigated the stereoelectronic properties of the metallocene frontier orbitals after the discovery that the one-carbon *ansa*-bridged compound (*cis*-η-butadiene)[(4-cyclopentadienylidene)-4,7,7-trimethyl-4,5,6,7-tetrahydroindenyl]zirconium exhibited similar properties to those observed for compounds **2** and **4** discussed above. Their Extended Hückel calculations led them to conclude that some late transition metal character was conferred on the zirconium by the lowering of the Cp–Zr–Cp angle, as a consequence of the change in energy of the $4a_1$ and b_2 valence orbitals, leading to an increase in π-character of the metal–ligand bonding ($2a_1$ and b_1 in their notation).

The compound [Zr{$Me_2C(\eta$-$C_5H_4)_2$}(*cis*-η^4-PhC_4H_4Ph)] (**5**) was prepared by treatment of *ansa*-bridged zirconocene dichloride with two equivalents of *n*-butyl lithium at −78 °C[18] followed by addition of 1,4-*trans,trans*-diphenylbutadiene to give ruby red crystals of **5** in *ca.* 75% yield. The proton ^{1}H NMR spectrum of **5** up to 50 °C showed no evidence for fluxional behaviour. The ^{1}H NMR spectrum showed a single resonance associated with the CMe_2 backbone and the presence of 4 signals assignable to η-C_5H_4 hydrogens, indicating either C_{2v} symmetry associated with the *trans*-isomer or C_s symmetry for the *cis*-isomer. COSY analysis shows that these signals correlate into two groups: those at δ 5.22 and 5.10 associated with one ring and those at δ 5.00 and 4.53 with the other. This

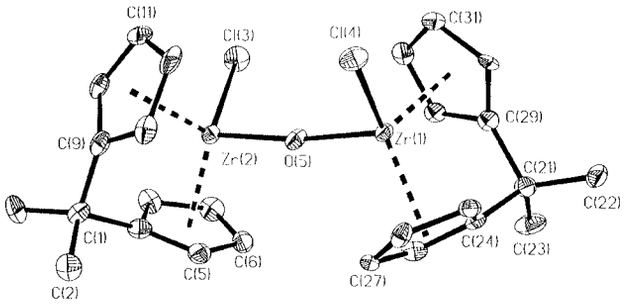

Fig. 6 Molecular structure of compound $[Zr\{Me_2C(\eta\text{-}C_5H_4)_2Cl\}_2\text{-}\mu\text{-}O]$ **6**.

implies that the *cis*-isomer is the predominant product, as does comparison of the butadiene proton chemical shifts with those of *cis*- and *trans*-$[Hf(\eta\text{-}C_5H_5)_2(\eta\text{-}PhC_4H_4Ph)]$[17] for which chemical shifts of 5.8 and 1.9 or 3.8 and 3.1 ppm are observed. These hafnocene–butadiene compounds show a marked preference for *cis*- rather than *trans*-coordination of the butadiene fragment, presumably due to the stronger M–C σ-bonds for third row transition metals compared to second row transition metals, and hence a preference for metallocyclopentene-type coordination. In this case, the *cis*-isomer predominates slightly at room temperature.

Treatment of a solution of $[Zr\{Me_2C(\eta\text{-}C_5H_4)_2\}(cis\text{-}\eta\text{-}C_4H_6)]$ **2** in THF with trichloroacetyl chloride Cl_3CCOCl gave colourless crystals of the binuclear $[Zr\{Me_2C(\eta\text{-}C_5H_4)_2Cl\}_2\text{-}\mu\text{-}O]$ (**6**). The oxygen is presumed to have derived from adventitious water. The X-ray crystal structure of compound **6** has been determined with the molecule crystallising in a monoclinic crystal system in the space group $P2_1/n$. The molecular structure is shown in Fig. 6, and selected interatomic distances and angles given in Table 7. The binuclear molecule **6** has an effectively linear Zr–O–Zr bridge and is very similar in structure to the unbridged zirconium[13] and cationic niobium[19] analogues. The Zr–O distances are short (1.95 Å), and are in the range of those found for terminal oxo-complexes, indicating a substantial amount of double bond character. This conclusion is supported by consideration of the torsion angle along the Cl–Zr–Zr–Cl bonds which is 104.8°. This angle is such that the sp-hybridised oxygen atom can use one of its p orbitals in π-bonding with each of the zirconium centres, thereby acting as a three-electron donor to each atom, and completing the 18-electron count of the metals. However the NMR evidence suggests that the molecule possesses horizontal mirror planes of symmetry through the zirconium atoms and, therefore, it appears that rotation about the Zr–O bond is occurring on the NMR timescale causing the symmetry to average to the expected D_{2h} where the chlorine atoms lie diametrically opposed to each other.

Erker and co-workers have shown that treatment of *cis*- and *trans*-isomers of $[Zr(\eta\text{-}C_5H_5)_2(\eta\text{-}C_4H_6)]$ with tris(pentafluorophenyl)boron results in addition of the $B(C_6F_5)_3$ group to the butadiene ligand and formation of zwitterionic η-allyl derivatives such as $[Zr(\eta\text{-}C_5H_5)_2\{\eta^3\text{-}CH_2CHCH_2[CH_2B(C_6F_5)_3]\}]$.[20] This prompted us to study the reaction between $B(C_6F_5)_3$ and **2**.

Addition of tris-pentafluorophenylboron in light petroleum ether (bp 40–60 °C) to compound **2** gave an orange powder $[Zr\{Me_2C(\eta\text{-}C_5H_4)_2\}\{\eta^3\text{-}C_4H_6B(C_6F_5)_3\}]$ (**7**). The solutions were thermally unstable and, after a period of 6 h, the NMR samples had to be replaced with freshly prepared solutions. The decomposition appears to be due to the production of a thermodynamically more stable isomer, as the new peaks which appear in the ^{1}H NMR spectrum correspond to a compound which was isolated and shown to possess the same empirical formula as compound **7**.

The ^{1}H NMR spectrum of **7** shows that the molecule lacks any elements of symmetry. Due to the difficulty involved in using a necessarily long acquisition time to obtain a proton decoupled ^{13}C spectrum, detection of the carbon signals by indirect methods was employed. The assignments were made using DQF-COSY and HSQC analysis to determine the connectivities. The high field signals at δ −0.25 and −1.13 and those at 2.73 and 0.94 are shown to arise from CH_2 groups, a far stronger coupling being observed between the latter pair implying sp^3-hybridisation of the associated carbon. These protons are also coupled to the low-field signal at 5.21 ppm; this shift could be due to distortion of the allyl group, increasing the $Zr\text{–}C_c$ bond length and deshielding the carbon atom which also resonates at comparatively low-field at δ 133.2. The large discrepancy in chemical shift between the two ends of the allyl group implies that the bonding is very much distorted towards σ,π-coordination, with the terminal carbon C_d acting as a σ-donor with coordination of the $C_b\text{–}C_c$ double bond to the metal centre in much the same way as in the metallocyclopentane mode of the *cis*-butadiene fragment.

The ^{11}B NMR spectrum of **7** shows a single resonance at δ −12.7 which is in accordance with a single tetra-coordinate boron atom. The ^{19}F spectrum of **7** at room temperature also shows the three characteristic signals at δ −135.9, −162.2 and −167.5 due to the *ortho*-, *para*- and *meta*-fluorine atoms, respectively. A marked change in the latter spectrum occurs upon cooling the sample; at −20 °C the *ortho*- and *meta*-signals begin to broaden, whilst the *para*-signal stays sharp down to −60 °C. This can be explained by assuming that the rotation of the ring about the $B\text{–}C_{ipso}$ bond is slowing down, thereby broadening the *ortho*- and *meta*-fluorine signals, but leaving the *para*-signal unaffected. This conclusion implies that rotation about this bond is slowed much more readily than that about the $C_d\text{–}B$ bond, as broadening of the *para*-signal is not observed until −65 °C. At this temperature the *ortho*-signal has split into several different resonances, one of which appears at a very high field (δ −216). This signal can be assigned to coordination of one of these fluorines to the zirconium centre, and thereby completing the 18-electron count of the metal centre. Splitting of the other two signals also starts to occur, but to a lesser extent. Spectra were recorded at temperatures down to −85 °C by which time many different resonances could be observed. However, due to limitations imposed by the solvent, a spectrum of the molecule which was "static" on the NMR timescale could not be obtained. These NMR data suggest the compound **7** to be $[Zr\{Me_2C(\eta\text{-}C_5H_4)_2\}\{\eta^3\text{-}C_4H_6B(C_6F_5)_3\}]$.

A freshly prepared solution of compound $[Zr\{Me_2C(\eta\text{-}C_5H_4)_2\}(cis\text{-}\eta\text{-}C_4H_6)]$ **2** in toluene was treated with $B(C_6F_5)_3$ and the solution changed from red to the yellow of compound **7**. This reaction mixture was then treated with an excess of trimethylphosphine to give pale yellow crystals of $[Zr\{Me_2C(\eta\text{-}C_5H_4)_2\}\{exo\text{-}\eta^3\text{-}C_4H_6B(C_6F_5)_3\}PMe_3]$ (**8**). The crystal structure of **8** was determined and the molecular structure is given in Fig. 7 and selected distances and angles are listed in the Table 8.

The compound **8** crystallises together with one molecule of THF in a monoclinic crystal system in a space group $C2/c$. The structure shows that the bulky $B(C_6F_5)_3$ and PMe_3 groups lie *trans* to each other. The four carbon atoms of the butadiene fragment are co-planar and lie in a *trans*-conformation. Bond

Table 7 Selected interatomic distances (Å) and angles (°) for $[Zr\{Me_2C(\eta\text{-}C_5H_4)_2Cl\}_2\text{-}\mu\text{-}O]$ **6**[a]

Zr(1)–O(5)	1.947(5)	Zr(1)–O(5)–Zr(2)	173.1(2)
Zr(2)–O(5)	1.947(4)	Cl(4)–Zr(1)–O(5)	99.67(12)
Zr(1)–Cl(4)	2.466(2)	Cl(3)–Zr(2)–O(5)	98.81(12)
Zr(2)–Cl(3)	2.467(2)	Cl(4)–Zr(1)–Zr(2)–Cl(3)	104.8
		CEN–Zr(1)–CEN	115.5
		CEN–Zr(2)–CEN	114.8

[a] The species co-crystallised with one molecule of diethyl ether per unit cell.

Table 8 Selected interatomic distances (Å) and angles (°) for compound [Zr{$Me_2C(\eta\text{-}C_5H_4)_2$}{*exo*-$\eta^3$-$C_4H_6B(C_6F_5)_3$}$PMe_3$] **8**

Zr(1)–C(30)	2.464(5)	C(30)–C(31)–C(32)	125.8(5)
Zr(1)–C(31)	2.527(5)	C(31)–C(32)–C(33)	123.8(5)
Zr(1)–C(32)	2.613(6)	C(32)–C(33)–B(34)	113.9(4)
Zr(1)–P(20)	2.748(2)	P(20)–Zr(1)–C(30)	70.8(1)
C(30)–C(31)	1.410(8)	Zr(1)–C(32)–C(33)	128.7(4)
C(31)–C(32)	1.384(8)	Zr(1)–C(32)–C(31)	71.0(3)
C(32)–C(33)	1.502(8)	Zr(1)–C(30)–C(31)	76.1(3)
Zr(1)–CEN(mean)	2.207	CEN–Zr(1)–CEN	116.0

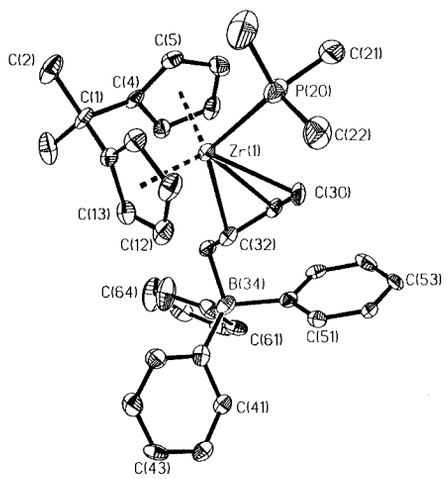

Fig. 7 Molecular structure of compound [Zr{$Me_2C(\eta\text{-}C_5H_4)_2$}{*exo*-$\eta^3$-$C_4H_6B(C_6F_5)_3$}$PMe_3$] **8**.

angles suggest that the atoms C(31) and C(32) are of approximately trigonal coordination, whilst the methylenic C(33) appears to be tetrahedrally coordinated. The bond lengths in the allyl group show the shortest distance is between the C(31) and C(32) carbon atoms. This is consistent with a stronger σ-interaction between C(30) and the metal, leaving substantial double bond character between the two remaining carbons which interact more weakly *via* a π-interaction with the zirconium centre. This is also reflected in the metal–carbon bond lengths, the C(30)–Zr(1) distance being markedly shorter than the other distances at 2.464(5) Å. Distortion of the allyl bonding is shown by these structural parameters; the Zr(1)–C(32) interatomic distance being over 2.6 Å, at the limit of the normal range for Zr–C distances. This distance is long enough to explain the low field-shifts observed for this nucleus and its associated proton in the NMR spectra, as a partial positive charge may be borne on this atom.

The low solubility of **8** prevented NMR spectra from being obtained in hydrocarbon solvents. For this reason NMR spectra were obtained in deuterated acetone in which the compound is freely soluble, but was observed to decompose slowly over a period of 12 h.

A freshly prepared solution of [Zr{$Me_2C(\eta\text{-}C_5H_4)_2$}{$\eta^3$-$C_4H_6B(C_6F_5)_3$}] **7** in toluene–pentane was treated with an excess of pyridine giving the compound [Zr{$Me_2C(\eta\text{-}C_5H_4)_2$}{*endo*-$\eta^3$-$C_4H_6B(C_6F_5)_3$}$C_6H_5N$] (**9**). Crystals of **9** were grown from a saturated THF solution which had been layered with pentane and the crystal structure was determined. The molecule **9** crystallised together with two molecules of THF in a monoclinic crystal system in a space group $P2_1/c$. The molecular structure is shown in Fig. 8, and selected interatomic distances and angles are given in Table 9. The pyridine ligand in the compound **9** is oriented *cis*- to the tris-pentafluorophenyl boron group. The four carbon atoms from the butadiene fragment are co-planar and in a *trans*-conformation. When compared to the structure of compound **8** it can be seen that the C(30)–Zr(1) bond length in **9** is reduced to 2.345(9) Å from 2.464(5) Å with a

Table 9 Selected interatomic distances (Å) and angles (°) for [Zr{$Me_2C(\eta\text{-}C_5H_4)_2$}{*endo*-$\eta^3$-$C_4H_6B(C_6F_5)_3$}$C_6H_5N$] **9**

Zr(1)–C(30)	2.345(9)	C(30)–C(31)–C(32)	122.5(9)
Zr(1)–C(31)	2.538(9)	C(31)–C(32)–C(33)	125.7(9)
Zr(1)–C(32)	2.81	C(32)–C(33)–B(34)	109.3(7)
Zr(1)–N(20)	2.394(7)	N(20)–Zr(1)–C(30)	126.4(3)
C(30)–C(31)	1.46(1)	Zr(1)–C(31)–C(30)	65.5(5)
C(31)–C(32)	1.37(1)	Zr(1)–C(31)–C(32)	86.9(5)
C(32)–C(33)	1.48(1)	Zr(1)–C(30)–C(31)	79.9(5)
C(33)–B(34)	1.66(1)	CEN–Zr–CEN	116.2

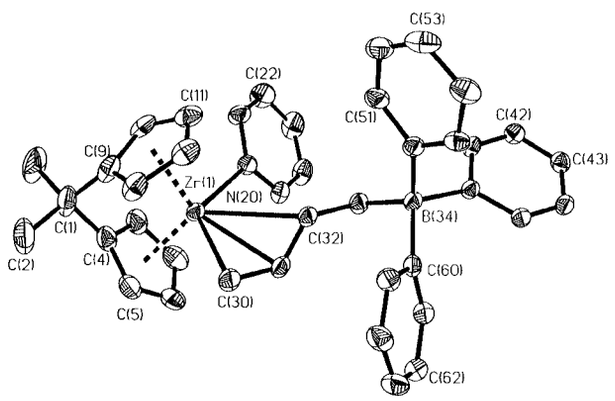

Fig. 8 Molecular structure of compound [Zr{$Me_2C(\eta\text{-}C_5H_4)_2$}{*endo*-$\eta^3$-$C_4H_6B(C_6F_5)_3$}$C_6H_5N$] **9**.

concomitant slight lengthening of C(30)–C(31) and shortening of the C(31)–C(32) bond distances.

A solution of compound **7** was treated with *tert*-butyl isocyanide, giving colourless microcrystals of [Zr{$Me_2C(\eta\text{-}C_5H_4)_2$}{*endo*- and *exo*-$\eta^3$-$C_4H_6B(C_6F_5)_3$}NC′Bu] (**10**). Further examination confirmed that two types of crystal were present, in the form of needles and plates. The major isomer shows similar features in its spectrum to those of both the PMe_3 and pyridine adducts, although protons H_b and H_c do in fact show more extreme chemical shifts. A considerable increase in intramolecular strain of an *endo*- rather than *exo*-form would be expected to contribute significantly to the increased range of chemical shifts. It is for this reason that this compound is tentatively assigned as the *endo*-isomer and the minor product as the *exo*-form where this effect is less pronounced.

Recrystallization of the mixture from diethyl ether produced colourless needles of the pure form of the minor product. This suggests that no interconversion of these two species is occurring in solution. Although the major product could not be isolated free from an impurity of the other isomer, different proportions of the two isomers could be obtained by crystallization from different solvents, supporting the above observation that the compounds are distinct and not due to precipitation of products from a dynamic equilibrium.

In conclusion, the new compounds and reactions are shown in Scheme 1. The presence of the *ansa*-bridge in the zirconocenes has a marked effect on the electronic properties at the zirconium centre compared to the non-*ansa* analogues.

Experimental

All preparations and manipulations of air and/or moisture-sensitive materials were carried out under an inert atmosphere of dinitrogen or argon using standard Schlenk line techniques or in an inert atmosphere dry box containing dinitrogen. Inert gases were purified by passage through columns filled with molecular sieves (4 Å) and either manganese(II) oxide suspended on vermiculite for the vacuum line or BASF catalyst for the dry box. Solvents and solutions were transferred through stainless steel cannulae, using a positive pressure of inert gas.

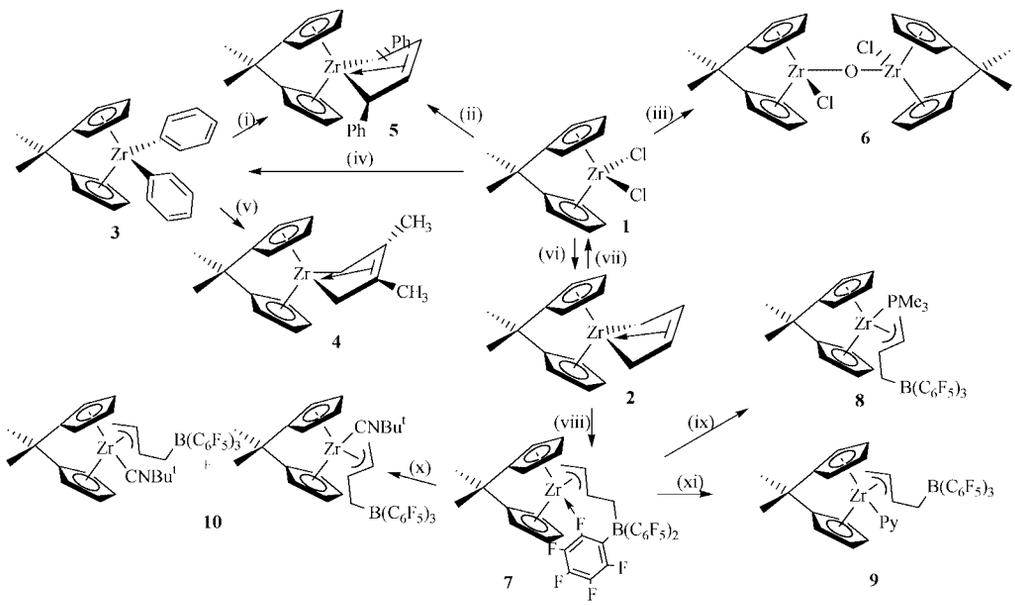

Scheme 1 (i) (a) $(Ph_2C_4H_4)Li_2$–toluene or (b) 2 *n*-BuLi, −78 °C followed by 1,4-diphenylbutadiene–THF, rt. (ii) 2 *n*-BuLi, −78 °C followed by 2 PhC_2Ph–THF, rt. (iii) Cl_3COCl, THF, rt. (iv) 2 PhMgBr–THF, −78 °C. (v) 2,3-dimethylbutadiene–toluene, *hν*, rt. (vi) $[(C_4H_6)Mg]_n$–toluene, rt. (vii) CH_3COCl–THF, rt. (viii) $B(C_6F_5)_3$–pentane, rt. (ix) PMe_3–toluene–light petroleum ether (bp 40–60 °C), rt. (x) CN′Bu–toluene–light petroleum ether (bp 40–60 °C), rt. (xi) Pyridine–toluene–light petroleum ether (bp 40–60 °C), rt.

Filtrations were similarly performed using modified stainless steel cannulae which could be fitted with glass fibre filter discs. All glassware and cannulae were thoroughly dried at 150 °C before use.

All solvents were thoroughly deoxygenated before use either by repeated evacuation followed by admission of dinitrogen or by bubbling dinitrogen through the solvent for approximately 15 min. Solvents were pre-dried over activated 4 Å molecular sieves and then distilled over sodium (toluene, petroleum ether bp 100–120 °C), sodium–potassium alloy (diethyl ether, *n*-pentane, light petroleum ether bp 40–60 °C), potassium (THF, benzene) or calcium hydride (dichloromethane, acetonitrile) under a slow continuous stream of dinitrogen. Perdeuterated solvents for NMR spectroscopy were deoxygenated and dried over calcium hydride (dichloromethane, acetonitrile) or potassium (benzene, THF and toluene) and then distilled before use. Celite 545 filtration aid (Koch-Light) was pre-dried at 140 °C and deoxygenated before use by repeated evacuation followed by admission of dinitrogen.

NMR spectra were recorded on either a Varian Unity Plus 500 (^{1}H, ^{11}B, ^{13}C, ^{19}F and ^{31}P NMR spectra were recorded at 499.868, 160.380, 125.704, 470.280, and 202.345 MHz respectively), or Bruker AM300 (^{1}H, ^{13}C and ^{31}P NMR spectra were recorded at 300.13, 75.5 and 121.6 MHz respectively). Indirect detection experiments were carried out on a Varian UnityPlus 500 fitted with a pulsed field gradient ID probe. The spectra were referenced internally using the residual protio solvent (^{1}H) and solvent (^{13}C) resonances and measured relative to TMS (^{1}H and ^{13}C; δ 0) or referenced externally to $BF_3{\cdot}Et_2O$ (^{11}B; δ 0), $CFCl_3$ (^{19}F; δ 0) or 85% H_3PO_4 (^{31}P; δ 0). All chemical shifts are quoted in δ and coupling constants are given in Hertz.

Electron Impact mass spectra were recorded on an AEI MS 302 mass spectrometer, updated by a data-handling system supplied by Mass Spectrometry Services Ltd. Fast Atom Bombardment mass spectra were obtained by the EPSRC Mass Spectrometry Service Centre at the University College of Swansea under the supervision of Dr J. A. Ballantine. Infrared spectra were recorded on a Perkin-Elmer 1710 FTIR spectrometer in the range 400 to 4000 cm^{-1} or a Matteson Instruments Galaxy series FT-IR 6020 spectrometer in the range 500 to 4000 cm^{-1}. Samples were either prepared as Nujol mulls between KBr plates, as KBr discs or as dilute solutions in a solution cell with KBr windows. Solution spectra were referenced to a blank cell containing only the solvent. All data given are in wavenumbers (cm^{-1}).

Photoelectron spectra were measured using a PES laboratories 0078 spectrometer interfaced with an Atari microprocessor. Spectra were calibrated with He, Xe and N_2.

Mass spectra were determined by the EPSRC Mass Spectroscopy Service Centre. Elemental analyses were obtained by the microanalysis department of the Inorganic Chemistry Laboratory.

All calculations were performed using density functional methods of the Amsterdam Density Functional package (Version 2.3).[18] The basis set used triple-ζ accuracy sets of Slater type orbitals, with relativistic corrections, with a single polarisation functional added to main group atoms; 2p on hydrogen and 3d on carbon atoms . The cores of the atoms were frozen; carbon up to the 1s orbital, and zirconium to the 3d orbitals. First order relativistic corrections were made to the cores of all atoms using the Pauli formalism. The GGA (non-local) method was used, using Vosko, Wilk and Nusair's local exchange correlation[21] with non-local-exchange corrections by Becke[22] and non-local correlation corrections by Perdew.[23] The non-local correction terms were not utilised in calculating gradients during geometry optimisations. The structures were constrained to *C5* symmetry. Vertical ionisation energies were estimated, using the optimised structure, from the difference between the total energy for the molecule and that for the molecular ion in the appropriate state.

Preparation of compounds

[Zr{$Me_2C(\eta\text{-}C_5H_4)_2$}(*cis*-η-$C_4H_6$)] 2. The compound [Zr{$Me_2C(\eta\text{-}C_5H_4)_2$}$Cl_2$] **1** (6.6 g, 20 mmol) and $Mg(C_4H_6){\cdot}2THF$ (4.64 g, 21 mmol) were weighed into a dried Schlenk tube, and toluene (100 ml) was added. The yellow suspension was stirred for 2 h until the solution had turned deep red in colour, and then for a further 2 h. The suspension was allowed to settle, and the red supernatant filtered off from the precipitate of $MgCl_2$ which was washed with toluene (25 ml) and the organic fractions combined. This solution was reduced in volume under reduced pressure to *ca.* 25 ml and allowed to crystallise at −80 °C for 2 days, giving red crystals of *cis*-[Zr{$Me_2C(\eta\text{-}C_5H_4)_2$}(η-$C_4H_6$)]. Yield 5.2 g (90%).

[Zr{$Me_2C(\eta\text{-}C_5H_4)_2$}$Ph_2$] 3. The compound [Zr{$Me_2C(\eta\text{-}C_5H_4)_2$}$Cl_2$] (7.2 g, 21.6 mmol) was dissolved in THF (50 ml) and the solution cooled to −78 °C. Aluminium foil was wrapped round the Schlenk tube to exclude light and phenyl magnesium bromide (3 M in diethyl ether, 14.6 ml, 44 mmol) added. The solution was slowly warmed to room temperature over a period of 1 h and the stirring continued for a further 12 h period during which time the yellow solution deepened in colour to light brown. The solvent was then removed under reduced pressure, and the residue washed with light petroleum ether (bp 40–60 °C) to leave a pale brown solid. Recrystallisation from toluene at −25 °C gave beige, light sensitive crystals of [Zr{$Me_2C(\eta\text{-}C_5H_4)_2$}$Ph_2$]. Yield 4.4 g (50%).

[Zr{$Me_2C(C_5H_4)_2$}(*cis*-η^4-$C_4H_4Me_2$)] 4. The compound [Zr{$Me_2C(\eta\text{-}C_5H_4)_2$}$Ph_2$] (100 mg, 0.24 mmol) was suspended in toluene (25 ml) and an excess of freshly distilled 2,3-dimethylbutadiene added (*ca.* 2 ml). The white suspension was irradiated with uv light for 15 h, by which time the reaction mixture had turned red/orange. Filtration followed by the removal of volatiles under reduced pressure gave a red residue consisting of an approximate 5:1 mixture of *cis*-[Zr{$Me_2C(\eta\text{-}C_5H_4)_2$}$(\eta\text{-}C_4H_4Me_2)$] and [Zr{$Me_2C(\eta\text{-}C_5H_4)_2$}$Ph_2$]. Recrystallisation from THF at −25 °C afforded large red crystals of the butadiene complex. Yield *ca.* 10 mg (8%).

***trans*,*trans*-1,4-Diphenylbutadiene dilithium salt.** The compound *trans,trans*-1,4-diphenylbutadiene (10 g, 49 mmol) was dissolved in THF (100 ml), and lithium shot (700 mg, 100 mmol) added under an atmosphere of argon. The mixture was placed in a sonication bath for two hours, during which time the solution turned a very deep metallic purple colour and the lithium metal was seen to dissolve. The solution was filtered and the solvent removed under reduced pressure to yield a dark green solid. This was shown to be the bis-THF adduct of the required product. Yield 17.3 g (95%).

[Zr{$Me_2C(\eta\text{-}C_5H_4)_2$}(*cis*-$\eta^4$-$PhC_4H_4Ph$)] 5. The compound $Li_2(PhC_4H_4Ph)\cdot 2THF$ (437 mg, 1.2 mmol) and [$Me_2C(C_5H_4)_2$-$ZrCl_2$] (400 mg 1.2 mmol) were weighed into a dried Schlenk tube which was placed in an ice bath. Toluene (20 ml) was added at its freezing point, and the mixture stirred whilst warming to room temperature. During this time the mixture darkened to a deep red colour. Stirring was continued for 6 h before the solvent was removed under reduced pressure. The red residue was extracted into petroleum ether (bp 100–120 °C), and the impurities removed by crystallisation at −25 °C. The filtrate was then cooled to −80 °C for 3 days, affording a dark red, thermally-sensitive powder of *cis*-[Zr{$Me_2C(\eta\text{-}C_5H_4)_2$}-($\eta^4$-$PhC_4H_4Ph$)]. Yield 112 mg (20%).

An alternative method of synthesis, analogous to the preparation of [Zr{$Me_2C(\eta\text{-}C_5H_4)_2$}($\eta^4$-$C_4H_4Me_2$)] was also employed. [Zr{$Me_2C(\eta\text{-}C_5H_4)_2$}$Ph_2$] (1 g, 2.4 mmol) was suspended in benzene (25 ml) and an excess of *trans,trans*-1,4-diphenylbutadiene added (*ca.* 2 g). The white suspension was irradiated with uv light for 25 h, by which time the reaction mixture had turned dark red in colour. Filtration followed by the removal of volatiles under reduced pressure gave a dark red residue consisting of a mixture of *cis*-[Zr{$Me_2C(\eta\text{-}C_5H_4)_2$}-($\eta^4$-$PhC_4H_4Ph$)], unreacted diphenylbutadiene and [Zr{Me_2C-$(\eta\text{-}C_5H_4)_2$}Ph_2]. Recrystallisation from THF at −25 °C afforded colourless crystals of the starting materials, whilst repeated crystallisations of the resulting supernatant gave pure *cis*-[Zr{$Me_2C(\eta\text{-}C_5H_4)_2$}($\eta^4$-$PhC_4H_4Ph$)]. This red powder could be observed to decompose over 6 h at room temperature to a bright yellow solid. Yield *ca.* 60 mg (5%).

A third method of synthesis was also employed. [Zr{Me_2C-$(\eta\text{-}C_5H_4)_2$}Cl_2] (332 mg, 1 mmol) was dissolved in THF (10 ml) and the solution cooled to −78 °C. *n*-BuLi (2 mmol) was added and the mixture stirred for 1 h. One equivalent of *trans-trans*-1,4-diphenylbutadiene in THF (5 ml) was then added and the mixture allowed to warm, with stirring, to room temperature over a period of 1–2 h. During this time a colour change from yellow to red could be observed. The solvent was then removed under reduced pressure and the residue extracted into toluene (30 ml) to produce a deep red solution, to which pentane (50 ml) was added and the product recrystallised as a deep red powder at −80 °C. Yield 335 mg, (75%).

Reaction of *cis*-[Zr{$Me_2C(\eta\text{-}C_5H_4)_2$}$(\eta\text{-}C_4H_6)$] with Cl_3CCOCl. The compound *cis*-[Zr{$Me_2C(\eta\text{-}C_5H_4)_2$}$(C_4H_4Me_2)$] (100 mg, 0.3 mmol) was dissolved in toluene (30 ml), and a solution of trichloroacetyl chloride in toluene added (0.3 mmol). The red solution immediately turned yellow with the deposition of a yellow precipitate over a period of 1 h. Precipitation was completed by the addition of light petroleum ether (bp 40–60 °C) (100 ml) and the supernatant liquor was filtered off. The resulting powder was recrystallised by dissolving in THF (5 ml) and layering with pentane (20 ml). Large yellow crystals were obtained over a period of 2 days which were shown by NMR and elemental analysis to be [Zr{$Me_2C(\eta\text{-}C_5H_4)_2$}$Cl_2$]. Yield *ca.* 90%.

Reaction of *cis*-[Zr{$Me_2C(\eta\text{-}C_5H_4)_2$}$(\eta\text{-}C_4H_6)$] with CH_3COCl: synthesis of [Zr{$Me_2C(\eta\text{-}C_5H_4)_2$l}$_2$-μ-O] 6. The compound *cis*-[Zr{$Me_2C(\eta\text{-}C_5H_4)_2$}$(C_4H_4Me_2)$] (320 mg, 1 mmol) was dissolved in THF (20 ml) and acetyl chloride (1 mmol) added. The solution was stirred for 12 h by which time the colour had changed from red to yellow. The volatiles were removed under reduced pressure to leave an oily precipitate. This was stirred vigorously with pentane (50 ml) for two hours to become a pale yellow powder which was isolated by filtration and dried *in vacuo*. This was then recrystallised from diethyl ether by slow cooling to −80 °C to give colourless crystals of [$(Me_2C(\eta\text{-}C_5H_4)_2ZrCl)_2$-μ-O]. Yield *ca.* 150 mg (56%).

[Zr{$Me_2C(\eta\text{-}C_5H_4)_2$}{$\eta^3$-$C_4H_6B(C_6F_5)_3$}] 7. The compound *cis*-[Zr{$Me_2C(\eta\text{-}C_5H_4)_2$}$(\eta\text{-}C_4H_6)$] (1 g, 3 mmol) was dissolved in toluene (50 ml) and a solution of $B(C_6F_5)_3$ in toluene (20 ml) added dropwise at −80 °C. The solution was allowed to warm to room temperature, with stirring over a period of two hours, during which time the solution had become orange. Pentane (250 ml) was then added, and the supernatant filtered off of the oily precipitate. This solution of [Zr{$Me_2C(\eta\text{-}C_5H_4)_2$}{$\eta^3$-$C_4$-$H_6B(C_6F_5)_3$}] was then immediately used in further reactions.

A pure sample of the solid for characterisation was prepared by dissolving *cis*-[Zr{$Me_2C(\eta\text{-}C_5H_4)_2$}$(\eta\text{-}C_4H_6)$]. (321 mg, 1 mmol) in light petroleum ether (bp 40–60 °C) (100 ml) and adding a solution of $B(C_6F_5)_3$ in light petroleum ether (bp 40–60 °C) (20 ml) dropwise over a period of 10 min. The solution immediately turned from red to orange, and an orange precipitate was deposited. The suspension was stirred for 30 min, and the supernatant filtered off. The precipitate was washed with light petroleum ether (bp 40–60 °C) (20 ml) and dried *in vacuo*, giving a yellow powder. Yield *ca.* 80%.

[Zr{$Me_2C(\eta\text{-}C_5H_4)_2$}{*exo*-$\eta^3$-$C_4H_6B(C_6F_5)_3$}$PMe_3$] 8. A saturated solution of [Zr{$Me_2C(\eta\text{-}C_5H_4)_2$}{$\eta^3$-$C_4H_6B(C_6F_5)_3$}] 7 (0.25 mmol) in pentane–toluene (4:1) was prepared as described above, and an excess of PMe_3 (*ca.* 1 ml) added to the orange solution. A fine white precipitate was deposited and allowed to settle. Filtration afforded a pale yellow powder which was recrystallised by dissolving in THF (5 ml) and layering with pentane (20 ml). Large pale yellow crystals of [Zr{$Me_2C(\eta\text{-}C_5H_4)_2$}{$\eta^3$-$C_4H_6B(C_6F_5)_3$}$PMe_3\cdot THF\cdot C_5H_{12}$] were formed as the layers diffused together. Yield *ca.* 200 mg.

[Zr{$Me_2C(\eta\text{-}C_5H_4)_2$}{*endo*-$\eta^3$-$C_4H_6B(C_6F_5)_3$}$C_6H_5N$] 9. This compound was synthesised by a method analogous to the preparation of [Zr{$Me_2C(\eta\text{-}C_5H_4)_2$}{$\eta^3$-$C_4H_6B(C_6F_5)_3$}$PMe_3$]

Table 10 Crystal structure data

	$(\mathbf{2})_2$[a]	**4**	**6**[a]·$(C_2H_5)_2O$	**8**[a]·(THF)	**9**·$(THF)_2$
Molecular formula	$C_{34}H_{40}Zr_2$	$C_{19}H_{24}Zr$	$C_{30}H_{38}Zr_2Cl_2O_2$	$C_{42}H_{45}BF_{15}OPZr$	$ZrC_{48}H_{41}BNF_{15}O_2$
Formula weight	631.10	343.62	683.94	983.78	1051.87
Crystal system	Monoclinic	Triclinic	Monoclinic	Monoclinic	Monoclinic
a/Å	7.623(9)	6.688(2)	16.106(3)	35.771(2)	11.724(2)
b/Å	15.203(15)	7.534(1)	8.853(2)	10.379(2)	17.331(6)
c/Å	23.029(20)	16.993(3)	21.598(4)	24.403(2)	22.963(9)
α/°		93.686(6)			
β/°	95.08(7)	95.980(7)	104.83(3)	116.940(5)	91.884(2)
γ/°		111.58(2)			
Volume/Å^3	2658.5(5)	786.9(5)	2977.0(10)	8076.8(2)	4663.1(3)
Space group	$P2_1/n$	$P\bar{1}$	$P2_1/n$	$C2/c$	$P2_1/c$
Z	4	2	4	8	4
Temperature/K	150	298	150	150	293
μ/mm^{-1}	0.806	0.68	0.904	0.416	0.32
Total data collected	9781	4164	4573	15498	9452
Unique data	3916	3783	4573	6006	7288
Merging *R* (%)	0.073	0.010	0.0401	0.0666	0.020
R	0.0363	0.0346	0.0426	0.0556	0.0612
R_w	0.0638	0.0342	0.0985	0.1274	0.0719

[a] Weighting scheme employed in least squares refinement $w = 1/[\sigma^2 (F_o^2) + (aP)^2 + bP]$ where $P = (F_o^2 + 2F_c^2)/3$. In all other cases the Chebychev polynomial weighting scheme was employed.[28]

above. A saturated solution of [Zr{$Me_2C(\eta$-$C_5H_4)_2$}{η^3-$C_4H_6B(C_6F_5)_3$}] (0.25 mmol) in pentane–toluene (4 : 1) was treated with an excess of pyridine (*ca.* 1 ml) with the immediate evolution of a white precipitate. This was isolated, washed with pentane (20 ml) and recrystallised as described above. Large pale yellow crystals were obtained after a period of 1 week, which were shown to be the *endo*-isomer of the compound [Zr{$Me_2C(\eta$-$C_5H_4)_2$}{η^3-$C_4H_6B(C_6F_5)_3$}C_5H_5N·2THF]. Yield 220 g (91%).

[Zr{$Me_2C(\eta$-$C_5H_4)_2$}{*endo*- and *exo*-η^3-$C_4H_6B(C_6F_5)_3$}NC^tBu] 10a,b. This compound was made in an analogous fashion to the PMe_3 adduct **8**: a saturated solution of [Zr{$Me_2C(C_5H_4)_2$}-{η^3-$C_4H_6B(C_6F_5)_3$}] **7** (0.25 mmol) in pentane–toluene (4 : 1) was prepared as described above, and an excess of $CNBu^t$ (*ca.* 1 ml) was added to the orange solution. A fine white precipitate was deposited over a period of 5 min after which time the stirring was stopped, and the precipitate allowed to settle. Filtration afforded a white powder which was washed with pentane (20 ml) and recrystallised by dissolving in THF (5 ml) and layering pentane (20 ml). Small colourless crystals were deposited over a period of several weeks, though on closer inspection these were seen to be of two distinct shapes, either needles or blocks. These were shown by NMR and elemental analysis to be the *endo*- and *exo*-isomers of [Zr{$Me_2C(\eta$-$C_5H_4)_2$}{η^3-$C_4H_6B(C_6F_5)_3$}CN^tBu]. A pure sample of the minor isomer was obtained by recrystallisation from toluene at −25 °C as pale yellow needles.

Crystal structure determination

Crystals of the compounds were mounted on a Nylon fibre using a drop of perfluoropolyether oil. They were rapidly cooled in a flow of cold nitrogen using an Oxford Cryosystems CRYOSTREAM cooling system. The crystal data are given in Table 10.

The data for **2** and **6** were collected on a Nonius FAST TV area detector diffractometer. The data were processed using MADNES[24] and refined using the SHELXS-86 and SHELXL-93 programs.[25] The data for **4**, **8** and **9** were collected on an Enraf-Nonius CAD4 and were processed using the program RC93.[26] Structures were solved by direct methods, SIR92[27] and CRYSTALS[28] (for **4** and **9**) and SIR92 and SHELXS-93 (for **8**). The hydrogen atoms were placed in calculated positions during the final cycles of refinement. A three parameter Chebychev weighting scheme[29] and corrections for anomalous dispersion were applied to all data. Neutral atom scattering factors were taken from International Tables for X-ray Crystallography.[30]

CCDC reference number 186/1767.

See http://www.rsc.org/suppdata/dt/a9/a908532g/ for crystallographic files in .cif format.

Acknowledgements

We thank the EPSERC for a grant (to G. C. T.). and Dr Simon J. Coles of the National Crystallography Laboratory.

References

1 L. Labella, A. Chernega and M. L. H. Green, *J. Organomet. Chem.*, 1995, **485**, C18.
2 L. Labella, A. Chernega and M. L. H. Green, *J. Chem. Soc.*, *Dalton Trans.*, 1995, 395.
3 A. Chernega, J. Cook, M. L. H. Green, L. Labella, S. J. Simpson, J. Souter and A. H. H. Stephens, *J. Chem. Soc.*, *Dalton Trans.*, 1997, 3225.
4 S. L. J. Conway, T. Dijkstra, L. H. Doerrer, J. C. Green, M. L. H. Green and A. H. H. Stephens, *J. Chem. Soc.*, *Dalton Trans.*, 1998, 2689.
5 G. Erker, C. Kruger and G. Muller, *Adv. Organomet. Chem.*, 1985, **24**, 1.
6 U. Dorf, K. Engel and G. Erker, *Organometallics*, 1983, **2**, 462.
7 G. Erker, J. Wicher, K. Engel and C. Kruger, *Chem. Ber.*, 1982, **115**, 3300.
8 H. Yasuda, Y. Kajihara, K. Mashima, K. Nagasuna, K. Lee and A. Nakamura, *Organometallics*, 1982, **1**, 388.
9 G. Erker, J. Wicher, K. Engel, F. Rosenfeldt, W. Dietrich and C. Krüger, *J. Am. Chem. Soc.*, 1980, **102**, 6344.
10 H. Yasuda, K. Tatsumi and A. Nakamura, *Acc. Chem. Res.*, 1988, **18**, 120 and references therein.
11 I. E. Nifant'ev, P. V. Ivchenko and M. V. Borzov, *J. Chem. Res.* (*S*), 1992, 162; I. F. Urazowski, I. E. Nifant'ev, K. A. Butakor and V. I. Ponomarev, *Metalloorg. Khim.*, 1991, **4**, 745.
12 S. S. Wreford and J. F. Witney, *Inorg. Chem.*, 1981, **20**, 3918.
13 J. F. Clarke and M. G. B. Drew, *Acta Crystallogr.*, *Sect. B*, 1974, **30**, 2267.
14 T. A. Albright, P. Hoffman and R. Hoffmann, *J. Am. Chem. Soc.*, 1976, **98**, 50.
15 J. C. Green, M. L. H. Green and C. K. Prout, *J. Chem. Soc.*, *Chem. Commun.*, 1972, 421; J. C. Green, *Chem. Soc. Rev.*, 1998, **27**, 283.
16 H. Yasuda, Y. Kajihara, K. Mashima, K. Nagasuna, K. Lee and A. Nakamura, *Organometallics*, 1982, **1**, 388.
17 T. Burghi, H. Berke, D. Wingbermuhle, C. Psiorz, R. Noe, T. Fox, M. Knickmeer, M. Berlekamp, R. Frohlich and G. Erker, *J. Organomet. Chem.*, 1995, **497**, 149.
18 E. J. Baerends and G. te Velde, *Theoretical Chemistry*, Vrije Universiteit, Amsterdam, 1997.

19 K. Prout, T. S. Cameron, R. A. Forder, S. R. Critchley, B. Denton and G. V. Rees, *Acta Crystallogr.*, *Sect. B*, 1974, **30**, 2290.
20 B. Temme, G. Erker, J. Karl, H. Juftmann, R. Fröhlich and S. Kotila, *Angew. Chem.*, 1995, **107**, 1867.
21 S. H. Vosko, L. Wilk and M. Nusair, *Can. J. Phys.*, 1980, **58**, 1200.
22 A. D. Becke, *Phys. Rev. A*, 1988, **38**, 3098.
23 J. P. Perdew, *Phys. Rev. B*, 1986, **33**, 8822.
24 A. Messerschmidt and J. W. Pflugrath, *J. Appl. Crystallogr.*, 1987, **20**, 306.
25 G. M. Sheldrick, SHELXS86 (1986) and SHELXS93 (1993), University of Göttingen, Federal Republic of Germany.
26 D. J. Watkin, C. K. Prout and P. M. deQ Lilley, Chemical Crystallography Laboratory, Oxford, 1994.
27 A. Altomare, G. Cascarano, C. Giacovazzo, A. Guagliardi, M. C. Burla, G. Polidori and M. Camalli, SIR 92, *J. Appl. Crystallogr.*, 1994, **27**, 435.
28 J. R. Carruthers, D. J. Watkin, *Acta Crystallogr.*, *Sect. A*, 1979, **35**, 698 and D. J. Watkin, C. K. Prout, R. J. Carruthers, P. Betteridge. CRYSTALS, 1996, Chemical Crystallography Laboratory, Oxford, England.
29 N. Walker and D. Stuart, *Acta Crystallogr.*, *Sect. A*, 1983, **39**, 158.
30 *International Tables for X-ray Crystallography*, vol. IV, Kynoch Press, Birmingham, 1974, Table 2.2B.

Paper a908532g